Wintertime sub-arctic new particle formation from Kola Peninsula sulphur emissions

Mikko Sipilä[1], Nina Sarnela[1], Kimmo Neitola[1], Totti Laitinen[1], Deniz Kemppainen[1], Lisa Beck[1], Ella-Maria Duplissy[1], Salla Kuittinen[1,2], Tuuli Lehmusjärvi[1], Janne Lampilahti[1], Veli-Matti Kerminen[1], Katrianne Lehtipalo[1,2], Pasi P. Aalto[1], Petri Keronen[1], Erkki Siivola[1], Pekka A. Rantala[1], Douglas R. Worsnop[1,3], Markku Kulmala[1], Tuija Jokinen[1], Tuukka Petäjä[1]

[1]Institute for Atmospheric and Earth System Research, PO. Box 64, 00014, University of Helsinki, Finland
[2]Finnish Meteorological Institute, 00560, Helsinki, Finland
[3]Aerodyne Research Inc. 01821 Billerica, MA, USA

Correspondence to: Mikko Sipilä (mikko.sipila@helsinki.fi)

Abstract. Metallurgical industry in Kola peninsula, North-West Russia, form a second largest source of air pollution in the Arctic and sub-Arctic domain. Sulphur dioxide emissions from the ore smelters are transported to wide areas including Finnish Lapland. We performed investigations on concentrations of SO_2 and aerosol precursor vapours, aerosol and ion cluster size distributions together with chemical composition measurements of freshly formed clusters at SMEAR I station in Finnish Lapland relatively close (~300 km) to Kola peninsula industrial sites during winter 2019-2020. We show that highly concentrated SO_2 from smelter emissions is converted to sulphuric acid (H_2SO_4) with sufficient concentrations to drive new particle formation hundreds of kilometres downwind of the emission sources even with very low solar radiation intensities. Observed new particle formation is primarily initiated by H_2SO_4 – ammonia (negative-) ion induced nucleation. Particle growth to cloud condensation nuclei (CCN) sizes was concluded to result from sulphuric acid condensation. However, airmass advection had a large role in modifying aerosol size distributions and other growth mechanisms cannot be fully excluded. Our results demonstrate the dominance of SO_2 emissions in controlling winter-time aerosol and CCN concentrations in the subarctic region with heavily polluting industry.

1 Introduction

Sulphur dioxide (SO_2) is one of the main air pollutants contributing to acidification of soils and freshwaters, defoliation and reduced vitality of forests, atmospheric aerosol and cloud formation as well as to millions of premature deaths globally. Anthropogenic SO_2 is primarily generated from the combustion of fossil fuels at power plants, other manufacturing complexes and ships, and smelting of sulphur containing mineral ores. Because of the severe environmental and health effects, efforts have been made in order to suppress SO_2 emissions. While the global emissions yet show no rapid decay, emissions in e.g. OECD countries have converged significantly within last 3 decades (Solarin and Tiwari, 2020).

The metallurgical industry with large scale smelter complexes in Kola peninsula, North-West Russia, form the second largest source of air pollution in the Arctic and sub-Arctic region. Smelters emit large quantities of SO_2, metals and particulate matter to the atmosphere. These pollutants, especially SO_2, largely impact the atmosphere and biosphere in the area, including eastern

35 parts of Finnish and Norwegian Lapland. In the close proximity of industrial plants these pollutants have literally destroyed ecosystems creating "industrial deserts" Paatero et al. (2008). Though emissions have significantly decreased from ca. 600 kilotons yr^{-1} in early 1990's (Tuovinen et al., 1993; Ekimov et al., 2001), partly because of the collapse of Soviet Union and related socio-economical changes in Russia, they are still high. Today, Kola peninsula SO_2 emissions are around 200 kilotons yr^{-1} (Barentz Observer, 2019), far higher than SO_2 emissions of the whole Finland (37 kilotons yr^{-1} in 2017). Though vast, Kola

40 emissions are still far behind the emissions of the World's number one SO_2 polluter, Norilsk (Krasnoyarsk Krai, Northern Siberia), with enormous 1.5 megatons yr^{-1} emission rates (Barentz Observer, 2019). Together with few other smaller scale industrial complexes these smelters are almost the sole local sources of air pollution in the very sparsely populated (sub-)Arctic Eurasia and therefore understanding their role in atmospheric chemistry and physics is of great importance.

45 SO_2 can be photochemically oxidized to sulphuric acid (H_2SO_4) in the gas phase. Though most of SO_2 reacts in liquid phase in cloud droplets and precipitate as acid rain, with very high concentrations of SO_2 in the Kola peninsula area also high production rate of gas phase H_2SO_4 can be expected. H_2SO_4 vapour can, in turn, contribute to atmospheric new particle formation (NPF) via nucleation and subsequent particle growth even up to sizes of cloud condensation nuclei (CCN) by further condensation of H_2SO_4 and potentially some other vapours (e.g. Weber et al., 1995; Kirkby et al., 2011; Jokinen et al., 2018). NPF is an

50 important process because, according to model simulations, it accounts for more than a half of atmospheric CCN formation globally (Merikanto et al., 2009; Gordon et al., 2017). In the high latitudes the contribution of NPF is estimated to be even larger, reaching >90% of the cloud level CCN in the high Arctic and approximately 70-80% in our study area, the sub-Arctic zone of Northern Finland and North-Western Russia (Gordon et al., 2017).

55 Vehkamäki et al. (2004) were first to report observations of NPF (> 8nm particles) at Värriö SMEAR I field station in eastern Lapland, Finland, relatively close to Kola peninsula smelter complexes. Their results on the contribution of SO_2 pollution were not completely definitive, out of four years of measurements and 147 observed NPF events 15 were concluded to be explained by the pollution plume. Kyrö et al. (2014) who recorded particle number size distributions down to 3 nm in diameter showed that NPF is connected to high concentrations of SO_2. They observed NPF even during winter in almost dark conditions,

60 indicating that during episodes of vast concentrations of SO_2 sufficient fraction is converted to H_2SO_4 in the gas phase even in very low solar radiation levels to initiate NPF. However, to date, no reports on quantification of sulphuric acid concentration by direct measurement or detailed mechanisms and chemical compounds involved in NPF in the area exists.

While observation of atmospheric NPF has been reported in hundreds of publications since the times of John Aitken (1900),
65 the details, i.e. the dynamics and contributing compounds, of NPF have been experimentally resolved only in a limited number

of atmospheric environments. Pioneering studies include observations by Weber et al. (1995) on the connection of between sulphuric acid and atmospheric nucleation, and the first report on ion-induced nucleation and simultaneous detection of sulphuric acid anion clusters by a mass spectrometer by Eisele et al., (2006). Among the field work, several laboratory investigations by the same research groups probed the properties of sulphuric acid – water and sulphuric acid – ammonia –
70 water clusters and their potential role in new particle formation (Ball et al., 1999; Hanson and Eisele, 2002).

Later advances in understanding the *molecular* steps of nucleation and growth in the atmosphere include the discovery that iodic acid (HIO_3) is primarily responsible on nucleation and growth in coastal areas and in the vicinity of the Arctic sea ice (Sipilä et al., 2016; Baccarini et al., 2020). Jokinen et al. (2018) demonstrated that in close coastal Antarctica, H_2SO_4 from
75 oxidation of dimethyl sulphide (DMS, emitted by pelagic phytoplankton) and ammonia (NH_3, from penguin colonies) nucleate via negative ion-induced mechanism with sulfuric acid condensation accounting for most of the subsequent particle growth. Further observations on nucleation mechanisms indicate the key role of highly oxidized organic molecules HOM (Ehn et al., 2014) in NPF in the spring-summer time boreal forest (e.g. Kulmala et al., 2013; Rose et al., 2018) and in the mid-latitude continental free troposphere (Bianchi et al., 2016) in parallel with sulfuric acid – ammonia nucleation (Bianchi et al., 2016;
80 Schobesberger et al., 2015; Yan et al., 2018). Dimethyl amine has been found to contribute to initial nucleation in polluted urban air (Yao et al., 2018). In addition to these, yet rare molecular level atmospheric observations several laboratory studies have investigated the details of these nucleation mechanisms (e.g. Kirkby et al., 2011; Almeida et al., 2013; Kürten et al., 2014; Kirkby et al., 2016).

85 Mass spectrometers (Junninen et al., 2010; Jokinen et al., 2012) and air ion spectrometers (Mirme & Mirme, 2013), have largely facilitated the recent progress in the field of atmospheric NPF. By utilizing them in conjunction with aerosol and meteorological observations, this work aims to shed light on the molecular steps of NPF resulting from (sub-)Arctic air pollution during wintertime. Investigations were carried out at SMEAR I research station in Värriö strict nature reserve in Finnish Lapland close to the industrial plants of Kola Peninsula, north-west Russia, during the winter 2019 – 2020.

90 **2 Methods**

2.1 Site and time of the study

Measurements were carried out at Värriö SMEAR I research station (Hari et al., 1994) located in Värriö strict nature reserve, Finnish Lapland, in the vicinity (5 km) of Russian border (Fig. 1) (67°45′19″N 29°36′37″E). Station is on top of a hill (390 m a.s.l.) and surrounded by untouched pine and spruce forests, bogs, fells, small lakes and rivers. Several large smelter complexes
95 are located close (~300 km) to the station on the Russian side of the border while on the Finnish side no smelters or other large-scale energy intensive (polluting) industrial plants are located within a distance of several hundreds of kilometres –

closest, relatively small, coal burning plant is 550 km away. SMEAR I station was set up in 1991 for monitoring the air pollution, especially sulphur dioxide (SO_2) originating from Kola peninsula smelters. In this work we present 4.5 months data from winter time, 1st November 2019 until 16th March 2020.

100 **2.2 Instrumentation**

Aerosol number size distribution between 3 and 750 nm was recorded by a twin differential mobility particle sizer (DMPS) (Aalto et al., 1999) comprising Hauke-type differential mobility analyzers (lenghts 110 and 280 mm) and TSI-3776 and TSI-3772 condensation particle counters (TSI Inc., Shoreview, MN, USA) as detectors. Another DMPS malfunctioned during 9th – 10th and 14th – 27th January resulting in the loss of data on 3 – 10 nm particles.

105

Number size distribution of charged particles and molecular clusters between 0.8 and 40 nm was recorded by a Neutral Cluster and Air Ion Spectrometer (NAIS, Airel Ltd., Estonia, Mirme & Mirme, 2013).

Aerosol precursor vapour concentrations, H_2SO_4, methane sulphonic acid (MSA), HIO_3 and HOM were measured by a nitrate

110 ion – Chemical Ionization -Atmospheric Pressure interface – Time-Of-Flight mass spectrometer (CI-APi-TOF, Jokinen et al., 2012) equipped from 26th January onwards with a switcher inlet, with which the instrument can switch between chemical ionization (CI) operation mode and natural ion detection mode. Instrument was calibrated in CI-mode for sulphuric acid as described by Kürten et al., 2012. Same calibration coefficient was used for reported MSA and HIO_3. Instrument was not operational at all times during the measurement campaign.

115

SO_2 was recorded with the TEI 43 i-TLE pulsed fluorescence analyzer, O_3 by the TEI 49 i photometric analyzer and NO_x by the TEI 42C TL chemiluminescence analyzer with photolytic NO_2-to-NO converter, all manufactured by Thermo Fischer Scientific (Franklin, MA, USA). Wind speed, direction and air temperature were measured with Vaisala WTX sensor 16 m above ground level.

120 **2.3 Nucleation rate calculation**

Negative (-) and positive (+) ion-induced nucleation rates of 1.5 nm particles, $J^{-/+}_{1.5}$, were calculated assuming a steady-state between formation and loss of particles in the size range of 1.5 and 2.5 nm:

$$J^{-/+}_{1.5} = \frac{dN^{-/+}_{1.5-2.5}}{dt} + \frac{GR_2}{\Delta d_p} N^{-/+}_{1.5-2.5} + CoagS\, N^{-/+}_{1.5-2.5} + k_{rec} N^{+/-}_{<1.5} N^{-/+}_{1.5-2.5} \qquad (1)$$

125

where $N^{-/+}_{1.5-2.5}$ is the total concentration of negative or positive ions in the size range between 1.5 and 2.5 nm, filtered using Matlab's Savitzky-Golay 2nd order filtering method with a frame size of 51 to remove instrument noice, k_{rec} is the recombination coefficient between negative and positive small ions which is here approximated by a size independent constant of $1.6 \cdot 10^{-6}$ cm³ s⁻¹ (Tammet, 1995), $N^{+/-}_{<1.5}$ is the concentration of positive or negative sub-1.5 nm cluster ions. GR_2 is the 2 nm particle

130   growth rate, width of the size interval for which concentration is defined Δd_p = 2.5 nm − 1.5 nm = 1 nm and $CoagS$ is the coagulation sink of 2 nm particles to background aerosol:

$$CoagS = \sum_{i=1}^{n} K_{2nm,i} N_i \qquad (2)$$

135   where N_i is the concentration of particles in the channel i of DMPS and coagulation coefficients $K_{2nm,i}$ between 2nm, and i nm particles are calculated based on Seinfeld and Pandis, 1998.

Accurate determination of particle growth rate for 2 nm particles from the size distribution is challenging, and therefore GR_2 was approximated by assuming irreversible sulphuric acid condensation (Stolzenburg et al., 2020):

140

$$GR_2 = \left(2.68 \cdot \left(\frac{d_p}{nm} \right)^{-1.27} + 0.81 \right) \cdot [H_2SO_4] \cdot 10^{-7} \, \text{molec.}^{-1} \, \text{cm}^3 \qquad (3)$$

as a sole mechanism of growth (Jokinen et al., 2018). Justification for the approach will be discussed later. More standard method for GR determination is to approximate GR_2 by the average growth rate of the formed particle population, including

145   mainly particles grown far above the 2 nm size, during a few hours starting from the beginning of the event as demonstrated in Supplement Figure S1. However, this approach neglects the effect of airmass advection which, as will be discussed later, may largely determine the time development of the size distribution and thus also the apparent growth. These two methods lead to a factor of ~17 difference in GR_2 on the example day depicted in Supplement Figure S1. For example, on example day of 29th January 2020 the factor of ~17 in GR_2 , is reflected in a factor of ~1.9 difference in the calculated nucleation rate. Ion-

150   induced nucleation rate calculation is thus not very sensitive to GR_2 because ion-ion recombination term dominates the loss in our conditions.

2.4 Sulphuric acid proxy calculation

Because of significant gaps in the measured data, $[H_2SO_4]$ was also calculated using a proxy developed by Dada et al. (2020). Calculation accounts for oxidation of SO_2 to H_2SO_4 both by OH (proxied by global radiation) and stabilized Criegee

155   Intermediates (Sipilä et al., 2014) proxied by monoterpene and ozone concentrations, as well as loss off H_2SO_4 by dimerization (negligible in observed concentrations) and condensation on pre-existing aerosol (the primary loss term). Unfortunately, there

are no VOC measurements available at SMEAR I, but because the data were collected during winter well outside of the growth period, we assumed monoterpene concentration to be zero. Global radiation measurement showed unexplained fluctuation (maybe caused by low solar zenith angles or freezing of the sensor) during the measurement period and therefore we used

160 UVB radiation and the relation between UVB and Global radiation determined by Dada et al. (2020).

2.5 Trajectory analyses

Trajectories were calculated by using the Hybrid Single-Particle Lagrangian Integrated Trajectory model HYSPLIT (Stein et al., 2015) with GFS 0.25 degree meteorology as an input. We calculated 24-hour backward trajectories arriving at 250 meters

165 above ground level, for the period 28.1.2020 00UTC to 30.1.2020 00 UTC, arriving every 6 hours. This is approximately the altitude at which SMEAR I station is and thus should represent the air that is also observed at the station even in a strong temperature inversion.

3 Results and Discussion

3.1 New particle formation during the measurement period.

170 Figure 2a depicts the aerosol size distribution between 3 and 800 nm as recorded by the DMPS. Several new particle formation events were recorded during the measurement period. Clear events where concentration of 4 -10 nm particles, N_{4-10nm}, (Figure 2b) exceeded 50 # cm^{-3} are marked with grey shading. Since DMPS data on sub 10-nm particles are missing from 9th -10th and 14th – 27th January N_{4-10nm} could not be derived for those time periods. Still, at least on 18th and 19th January NPF above 10 nm takes place. Events mostly coincided with eastern (~90°) winds (Figuge 2c) and elevated H_2SO_4 concentrations (Figure 2d)

175 calculated based on Dada et al. (2020). H_2SO_4 concentrations depend besides condensation sink and UVB radiation, on SO_2 concentration which is connected to wind direction and airmass origin. Clear examples of such, SO_2 pollution driven events are for example those occurring during three consequent days between 10th -12th November, 2019, two days on 28th – 29th January, 2020 and 13th March, 2020. Data from 28th – 29th January are discussed in detail while data from the other two exemplary event periods are presented in the Supplement (Figures S2 – S7).

180

Not all events occurred during eastern winds. The events observed close to mid-winter, from early December until early January, occurred with western winds or during the transition of wind direction from west to east, in relatively low concentration of SO_2 and virtual absence of day light and H_2SO_4. These low-H_2SO_4 mid-winter events are observed to start from sizes larger than few nm, i.e. nucleation does not take place in-situ in the surroundings of SMEAR I. Those particles thus

185 have formed elsewhere and transported to the measurement site by horizontal advection or vertically down from above the mixed layer. While new particles, with diameters of few nanometres, can survive a while against loss by coagulation, H_2SO_4

is lost much more rapidly to pre-existing particles after its production ceases. Therefore, the lack of H_2SO_4 is not excluding its primary role in NPF though not supporting that role either. Some of the mid-winter events coincide with elevated SO_2, suggesting that sulphuric acid may have be formed in the airmass earlier, while some, especially the relatively strong event on
190 December 3rd presented in the Supplement (Figures S8-S10) occurs in the virtual absence of SO_2 suggesting that sulphuric acid has not been formed to significant extent in that airmass. Currently we thus cannot explain the mechanism of NPF that day. However, the NO_2 concentration is slightly (Figure S8) elevated in the air mass, which might be connected to the event or source of particles. Nevertheless, most of the events seem to be connected to the presence of H_2SO_4.

3.2 Case study $28^{th} – 29^{th}$ January 2020

195 To resolve the details of new particle formation and growth, we focus on 3 time periods with clearly occurring nucleation and particle growth. Here we show results from analysis of a 2-day period from $28^{th} – 29^{th}$ January 2020. To demonstrate that the discussed 2-day period is not only a unique observation, we represent data from time periods of 10th -12th November, 2019 (Figures S2-S4) and 13th March, 2020 (Figures S5-S7) in the Supplement. Data from the reasonably strong event on 3rd December, 2019, which differs from the overall picture are also depicted in the Supplement (Figures S8-S10).

200 ### 3.2.1 Meteorological situation and trace gas concentrations

Throughout the period of $28^{th} – 29^{th}$ January the wind was blowing from the East (~50 - 150°) (Figure 3a). Temperature ranged from -16°C to -28°C (Figure 3b). Sky was clear but because of the small solar zenith angle (maximum 4.4° at noon 29th Jan.), UVB radiation intensity, needed for photochemical H_2SO_4 formation, reached only 35 mW m^{-2} (summertime UVB radiation intensity maxima at Värriö are >2000 mW m^{-2}). HYSPLIT back trajectory calculations show that airmasses arriving between
205 January 28th 6:00 – January 30th 00:00 passed the industrial areas of Montchegorsk region (Figure 4).

Around 3:00 on 28th January coinciding with the change in airmass origin to Montchegorsk – Kandalaksha region (Figure 4) (a few hours after the change of wind direction from west to east in the evening of 27th January), air pollutant levels started to increase steeply (Figure 3d). During the course of the day both SO_2 and NO_2 concentrations increased several orders of
210 magnitude with [SO_2] peaking at 27 ppb and [NO_2] at 7 ppb. Ozone (O_3) concentration declines from ca. 40 ppb to 30 ppb range. To give perspective to the high level of SO_2 concentration, the highest concentration recorded at Helsinki Metropolitan area was 8.4 ppb (24 µg m^{-3}, 1-hour average) in the year 2019 and the yearly average concentration was ca. 0.2 ppb (~0.5 µg m^{-3}) (Helsinki Region Environmental Services Authority, 2020). The yearly average concentrations at SMEAR I in 2019 was 1.1 ppb.

3.2.2 Aerosol precursors

Despite the low UVB radiation, required for O_3 photolysis that initiates H_2SO_4 production via OH radical formation, H_2SO_4 concentration increases from close to lowest detection limit values of $\sim 10^5$ molecules cm^{-3} up to $8 \cdot 10^5$ molecules cm^{-3} during 28th and up to $1.5 \cdot 10^6$ molecules cm^{-3} on 29th (Figure 5e). Because OH production rate must be low, high SO_2 concentration is a perquisite for the H_2SO_4 production during cold and dark winter months. Though stabilized Criegee Intermediates (sCI) formed in alkene ozonolysis can oxidize SO_2 to produce H_2SO_4 during summertime (Mauldin et al., 2012; Sipilä et al., 2014), alkene (terpene) emissions from the vegetation and thus sCI production rate are negligible during the winter season. Proxy calculations agree well with the measured sulphuric acid concentration on 29th but show clearly higher values on 28th January. The cause of the disagreement on 28th January is probably the stable and shallow boundary layer. Temperature gradient close to surface is almost +0.2 °C m^{-2} at noon on 28th (Figure 3b). Solar radiation from close the horizon is not penetrating efficiently inside the canopy and thus UVB measured above canopy and used in the proxy calculation does not reflect the situation at the ground level. Sulphuric acid produced above the canopy, on the other hand, does not mix downwards due to strong temperature inversion and calm wind. On 29th January the gradient is absent or slightly negative allowing surface air to mix with the air above canopy.

Besides H_2SO_4, also minute signals of iodic acid (HIO$_3$) is observed during the day (Figure 5e). The exact production mechanism of HIO$_3$ remain globally unknown despite the emerging evidence on its critical role in new particle formation especially in the Arctic regions (Sipilä et al., 2016; Baccarini et al., 2020). Methane sulphonic acid (MSA), that has been observed in larger aerosol particles (refs.) and that could potentially contribute also to NPF, hardly exceeds the detection threshold. This was expected since MSA originates from dimethyl sulphide (DMS) photo-oxidation. DMS end up in the air mainly from metabolism of pelagic phytoplankton during summer months, not during dark winter. No other condensable vapours, such as HOM which dominate the new particle growth in summertime boreal forest (Ehn et al., 2014), were observed during this case study period or during other periods depicted in Supplement.

3.2.3 New particle formation

Ion size distribution

Figures 5a&b show the NPF events on 28th and 29th January as observed by NAIS operated in ion mode. Omnipresent small < 1.5 nm ions are continuously produced by galactic cosmic radiation and radon decay. Approximately at 11 o'clock on 28th January, coinciding with the increase of H_2SO_4 concentration, small negative cluster ions start to grow, which is seen as small increase in $\sim 1.5-2$ nm negative ion concentration. During their growth beyond ~ 2 nm in diameter, those cluster are neutralized by collisions with positively charged ions and thus they disappear from the spectrum. They still obviously continue their growth

since charged particles reappear in the spectrum after reaching some 5 nm in diameter when diffusion charging becomes effective enough; equilibrium charging state for 2 nm particles is 0.8% while 5 nm particles are charged with an efficiency of 2.3% and out of 20 nm particles 11% are negatively charged (Wiedensohler et al., 2012). Opposite to negative ions, positive cluster ions do not grow. Larger, > 5nm positive particles (charged by diffusion charging during the course of their growth)

250 grow similar to negative particles. On 29th January, with clearly higher H_2SO_4 concentration, the appearance of >1.5nm negative clusters is more pronounced suggesting higher rates of nucleation and critical role H_2SO_4 in the initial steps of NPF. Positive cluster ions are again only bystanders and do not contribute to nucleation. This observation suggests negative ion-induced nucleation as a primary pathway to new particle formation similar to $H_2SO_4 - NH_3 (- H_2O)$ ion-induced nucleation observed by Jokinen et al. (2018) in Antarctica and Kirkby et al. (2011) in CERN CLOUD chamber experiments.

255

Nucleation rates

Even though weak growth of the small negative ions around noon on 28th January is visually observable in Figure 5a the concentration of clusters in the $1.5 - 2.5$ nm size range ($N^-_{1.5-2.5}$) is hardly distinguishable from the noise (Figure 5c). Nucleation

260 rate, calculated using filtered concentration data, only slightly exceeds the baseline (caused by presence of minute, almost omnipresent signal from ion clusters extending above 1.5 nm but which is not connected to sulphuric acid nucleation), and is approximately $0.005 \ cm^{-3} \ s^{-1}$ with high relative uncertainty (Figure 5d). On 29th, with 2.3-fold sulphuric acid concentration, the concentration of $1.5 - 2.5$ nm negative clusters is well above the instrument noise reaching $20 \ cm^{-3} \ s^{-1}$ around noon. Nucleation rate peaks at $0.064 \ cm^{-3} \ s^{-1}$. Temperatures during nucleation (~ noon) were close identical, around $-22°C$, in both days and

265 therefore they can be directly compared. Approximately 10-fold difference in nucleation rate between the two days and a factor of 2.3 difference in sulphuric acid concentration is in line with the results from the CLOUD-chamber experiment on sulphuric acid – ammonia – water nucleation (Kirkby et al., 2011). The so-called "slope" that approximately (not exactly in real atmospheric situations) equals to the number of sulphuric acid molecules in the critical cluster (Vehkamäki et al., 2012) is given as:

270

$$Slope = \frac{d \log J^+_{1.5}}{d \log [H_2SO_4]}$$

and yields a value of 2.9 for above discussed values. Though the value is subject to significant uncertainty it would agree with observations of Kirkby et al. (2011) who reported a "slope" of approximately 3 under close similar conditions ($-30°C$, in

275 presence of galactic cosmic radiation, sulphuric acid and <50 ppt ammonia). The sources or concentration of ammonia in our study area are not known.

Cluster time series

280   To confirm the role of sulphuric acid and to solve the contribution of ammonia in the nucleation process, we measured the negative ion cluster composition and signal intensity with the APi-TOF in ion mode without chemical ionization. Time series of most abundant clusters show the appearance of HSO_4^- - ion in the morning of 28th Jan together with increasing $[H_2SO_4]$ accompanied with a decay of NO_3^- - ion which typically dominates the anion spectrum at low $[H_2SO_4]$ and low $[HIO_3]$ globally (Figure 5f). Since H_2SO_4 is a stronger acid than HNO_3, proton transfers from H_2SO_4 to NO_3^- explaining the observed behaviour

285   when $[H_2SO_4]$ starts to rise. When $[H_2SO_4]$ still increases during the course of the day, $(NH_3)_m(H_2SO_4)_nHSO_4^-$ - clusters start to form. Cluster signals peak around noon coinciding with the highest $[H_2SO_4]$ and $N^-_{1.5\text{-}2.5}$ after which they start to decay. On 29th January, the same behaviour is observed, but with somewhat stronger cluster signals due to the higher $[H_2SO_4]$.

Cluster composition

290

To get more insight into the chemical composition of clusters, the ion-cluster mass spectrum was integrated over 4 hours (2 hours effective data collection due to switching between CI and ion-inlet). The resulting spectrum is presented in Figure 6 by means of a mass defect plot, where the mass-to-charge ratio (m/z, unit Th) corresponds – with only singly charged ion clusters present in the air – to the mass of the cluster (m, unit Da, equal to unified atomic mass unit, u). Mass defect is the mass

295   difference (in Th or Da) between the exact mass of the cluster and the integer mass defined as the sum of nucleons in the atomic nuclei of the cluster; for example, exact mass of a HSO_4^- -ion that has 97 nucleons is 96.960103 Da and the mass defect is thus 0.039896 Da. Area of the dot is proportional to the logarithm of the observed signal intensity. In the mass defect plot each addition of a molecule or atom is represented by a vector. Addition of, e.g., H_2SO_4, with a negative mass defect leads to increasing mass and decreasing total mass defect, while an addition of a positive mass defect NH_3 molecule leads to increasing

300   total mass defect. Successive addition of certain molecules to an ion results into a straight line in the defect plot so that the different cluster formation pathways are readily distinguishable from the plot.

Largest signals are associated with omnipresent nitrate ion and its cluster with nitric acid (NO_3^- and $HNO_3 \cdot NO_3^-$). Rest of the small (<180 Da) ions are mainly different sulphur species, with bisulphate ion partly clustered with nitric acid (HSO_4^- and

305    $HNO_3 \cdot HSO_4^-$) being most abundant. Other small sulphur ions present in the spectrum are SO_4^-, SO_5^-, $HNO_3 \cdot SO_3^-$ and $HNO_3 \cdot SO_4^-$. Deprotonated iodic acid (IO_3^-) and its nitric acid cluster, ($HNO_3 \cdot IO_3^-$) are also abundant. Despite multiple different types of these core ions, initial growth of them is solely caused by the attachment of sulphuric acid molecules. We observed clusters with 1-4 H_2SO_4 molecules attached to SO_4^- - ion, one H_2SO_4 molecule to SO_5^- and SO_3^- - ions and 1-3 H_2SO_4 molecules to IO_3^- -ion. For simplicity, we assume that the negative charge remains in the core ion. This is not necessarily true, but H_2SO_4

310   may lose a proton e.g. to IO_3^- resulting in composition of $HIO_3 \cdot (H_2SO_4)_{n-1} \cdot HSO_4^-$ instead of $^-(H_2SO_4)_n \cdot IO_3^-$. Furthermore, water,

if present in the clusters, efficiently evaporates in the vacuum of the mass spectrometer and therefore information on the role of water in the cluster formation is lost.

None of the above discussed clusters seem to adopt ammonia efficiently enough for their signals to exceed the detection
315 threshold of the APi-TOF (mass dependent, $\sim 10^{-3}$ to few 10^{-3} ions/second for 2 hour integration for m/z > 400 Th). Only clusters made solely of sulphuric acid with a bisulphate ion (HSO_4^-) as a core seem to efficiently attach ammonia resulting in the formation of $(NH_3)_m \cdot (H_2SO_4)_n \cdot HSO_4^-$ -clusters (n>=3). This sequential addition of NH_3 and H_2SO_4 has been shown to be an effective (ion-induced) cluster formation and growth mechanism in coastal Antarctica (Jokinen et al., 2018) as well as a secondary pathway in the free troposphere (Bianchi et al., 2016) and in the spring/summer time southern Finland boreal forest
320 (Yan et al., 2018).

Our results on negative cluster composition can be compared to the results from CLOUD experiment at -25°C for varying NH_3/H_2SO_4 - ratio (Schobesberger et al., 2015). Based on those data, with the NH_3/H_2SO_4 - ratio exceeding approximately 100 the cluster composition, and also the nucleation rate (Kirkby et al., 2011), saturate and become unaffected by the increase of
325 NH_3-concentration. In those conditions a cluster comprising 3 molecules of sulphuric acid on a bisulphate ion, $(NH_3)_n \cdot (H_2SO_4)_3 \cdot HSO_4^-$, contains on average approximately n~1 molecule of ammonia and cluster composed of 4 molecules of sulphuric acid and a bisulphate ion, $(NH_3)_n \cdot (H_2SO_4)_4 \cdot HSO_4^-$, carries on average approximately n~1.5 NH_3 molecules (Schobesberger et al., 2015). In our case (Figure 6), corresponding average ammonia numbers are n~0.4 and n~0.8 for $(NH_3)_n \cdot (H_2SO_4)_3 \cdot HSO_4^-$ and $(NH_3)_n \cdot (H_2SO_4)_4 \cdot HSO_4^-$, respectively, suggesting that NH_3/H_2SO_4 – ratio in our case is well below
330 100, likely below 10 (Schobesberger et al., 2015). That would indicate ammonia concentration of the order of $\sim 10^7$ molecules cm^{-3}, or ~1 pptv. Low NH_3/H_2SO_4 – ratio would mean that the system is not saturated with respect to NH_3 and the nucleation rate should therefore be sensitive to both H_2SO_4 *and* NH_3 similar to Jokinen et al. (2018). This highlights the importance of understanding NH_3 sources, transportation and atmospheric mixing ratios down to sub-ppt levels for a proper description of new particle formation also in the subarctic region. Unfortunately, NH_3 concentrations in the range of 1 pptv are not (reliably)
335 detectable with any present-day measurement technology.

The present analysis shows that sulphuric acid – ammonia ion-induced nucleation can trigger new particle formation in the winter time sub-arctic / boreal environment with high level of anthropogenic SO_2 pollution but low UV-radiation intensity. Data on neutral 1.5 - 3nm particles are not available and neutral nucleation rates could not be derived. However, based on all
340 evidence obtained from field (mainly Jokinen et al., 2018) and especially from CLOUD experiments (Kirkby et al., 2011; Schobesberger et al., 2015), in absence of significant amounts of compounds other than H_2SO_4 and NH_3 and with nucleation rate below the ion pair production rate (typically 2-4 ion pairs cm^{-3} s^{-1} in the Earth's surface layer) ion induced nucleation dominates over the neutral process. In our case, HOM were below the detection limit, and amines, if important, would appear

also in the anion spectrum in H$_2$SO$_4$ clusters. HIO$_3$ and MSA were present, but significant neutral homogeneous nucleation of
345   HIO$_3$ would require ~100-fold concentration (Sipilä et al., 2016).

The observation of clusters containing IO$_3^-$ or HIO$_3$ together with H$_2$SO$_4$ is, however, highly interesting. HIO$_3$ has been shown
to nucleate homogeneously but no reports on mixed clusters containing both HIO$_3$ and H$_2$SO$_4$ exists though Sipilä et al. (2016)
found unidentified sulphur compounds in the ion cluster population dominated by iodic acid in the Atlantic coast. If the SO$_2$
350   rich pollution plumes are advected to iodine source areas (arctic ocean and especially sea ice zone as well as macroalgae rich
coasts) or vice versa, this mixed mechanism may become important.

3.2.4 Particle growth and relevance for CCN-concentrations

Based on the above analysis, particle nucleation is clearly driven by sulphuric acid and ammonia with nucleation rate sensitive
to concentrations of both. But how do the freshly nucleated clusters grow? Assuming irreversible condensation, even the peak
355   sulphuric acid concentration of 1.5·10^6 molecules cm^{-3} can explain only a small fraction of the observed growth rate. Consistent
with an earlier report on wintertime particle growth rates at Värriö (Kyrö et al., 2014), the apparent average growth rate on
29th January is approximately 4.5 nm h^{-1} (Figure S1), which, based on Stoltzenburg et al. (2020) would require a steady
concentration of ca. 2.6·10^7 molecules cm^{-3} throughout the growth process which continues long after the sunset and the decay
of [H$_2$SO$_4$]. Obviously, there are two possibilities for the disagreement. Either sulphuric acid is not responsible for most of the
360   growth or the air is not homogenous and the apparent growth is caused by the airmass advection.

Besides sulphuric acid, only condensable vapours detected are MSA and HIO$_3$ (and NH$_3$). However, their concentrations are
clearly lower than that of sulphuric acid, and therefore condensation of those in a homogeneous airmass cannot explain the
apparent growth either. It could be speculated that compounds not recorded by CI-APi-TOF, such as SO$_2$ or some volatile or
365   semi-volatile organic compounds, (S)VOC, react in particle phase forming low volatile compounds therefore contributing to
growth but we have no evidence on such a process. NO$_2$ concentration was moderate, up to 7 ppb, and therefore also nitric
acid concentrations were likely insufficient to have a measurable effect on growth (Wang et al., 2020). However, temperature
was low during the studied time period and therefore HNO$_3$ or some contribute to growth, if they were present. Ammonia was
detected in small ion clusters but its contribution to particle volume, assuming the cluster NH$_3$/H$_2$SO$_4$ -ratio reflects the
370   composition of also larger particles, is marginal. Assuming particle composition to be ammonium bisulphate, i.e. NH$_3$/H$_2$SO$_4$
-ratio of unity, ammonia would contribute 17% to the particle volume and 5% to particle diameter growth rate.

The most plausible explanation for the observed growth is that the particle growth is driven by H$_2$SO$_4$ condensation but its
concentration is not uniform over the source area. In that case, particles would nucleate and grow to their final size during the
375   few hours of sunlight. Particles formed and grown in the close proximity of emissions source in high SO$_2$ and thus H$_2$SO$_4$

concentration environment grow to larger sizes than particles that are formed near the measurement site. Airmass advection would then transport particles through the dark hours leading to steadily increasing nucleation (and later Aitken) mode diameter at SMEAR I observed as apparent steady growth even through the night. Modelling efforts and measurement of chemical composition or hygroscopicity of growing mode would be required for unambiguous explanation of the particle growth.

380

New particle formation in the sub-Arctic winter would be irrelevant if formed particles would not grow to sizes (above few ten nm) where they can act as CCN. CCN concentrations (in different supersaturation) were not recorded but the airmass arriving from the Murmansk – Kandalaksha region from 28th January ca. 3:00 onwards (Figure 4) contains elevated concentration of Aitken and accumulation mode particles mainly in the size range of ~20 – 500 nm (Figure 7). New particle
385 formation clearly increases the concentration of >3 nm particles but also the concentration of particles larger than 50 nm show increase especially on 29th January. >100 nm particle concentration is relatively constant and apparently unaffected by the NPF in the time scale the events could be observed. Airmass advection, and particle loss processes, however, naturally have an impact on measured concentrations and are largely responsible on development of particle populations.

390 Figure 8 presents the average particle number size distribution during the ca. 1-week period of eastern winds (28th Jan – 3rd Feb 2020) when the two clear NPF events presented above occurred. Concentrations of particles in all size classes were remarkably higher, even an order of magnitude for 10-200 nm particles, than the average concentrations during the preceding and succeeding time period with western winds. Concentrations during that 1-week period were also clearly higher the average concentrations between 1st November and 29th February suggesting that new particle formation may be a significant source of
395 particles in the eastern airmasses. However, primary emissions from smelters and the surrounding cities would naturally show up in the size distribution plot as well. More thorough analysis is needed to separate the roles of secondary NPF and primary emissions in the aerosol and CCN budgets. For clarity March, with almost constant NPF is excluded from this analysis.

Since the observed secondary particles are probably highly acidic, they are also highly hygroscopic extending the CCN active
400 fraction toward smaller particle sizes. For accurate assessment of contribution of secondary aerosol formation in CCN concentrations at SMEAR I or regionally, meteorological situation, including boundary layer dynamics, wet deposition of particles, etc. should be accounted for. However, our observations point toward a major contribution of Kola peninsula SO_2 emissions to winter time CCN concentrations in the region.

4 Conclusions

405 Winter time secondary new particle formation and growth was investigated at SMEAR I station, in Värriö strict nature reserve, Finnish Eastern Lapland. Sulphur dioxide concentration in the airmasses arriving from Kola peninsula were often very high,

occasionally over 30 ppb. In these high concentrations enough sulphuric acid formed even in very low solar radiation intensity to initiate new particle formation and growth.

410 New particle formation was observed mostly, but not solely, with eastern winds and in airmasses arriving from the direction of Kola peninsula smelters. Newly formed (4-10 nm, concentration > 50 # cm^{-3}) particles were observed in altogether 51 days between 1st November 2019 and 31st March 2020. Excluding March, these signs of new particle formation were observed in 30 days. Nucleation was observed in-situ at SMEAR I during events associated with H_2SO_4 concentration exceeding ca. $1\cdot10^6$ molec. cm^{-3}. These cases were identified based on the appearance of ~1.5-2 nm ion clusters. Other events were observed as

415 appearance of few nm particles which gradually grew over time. Nucleation at SMEAR I was shown to proceed primarily via negative ion-induced sulphuric acid – ammonia (– water) channel. Closer to SO_2 emission sources where H_2SO_4 concentrations are likely remarkably higher, nucleation can proceed also via neutral channel and could, theoretically, involve compounds other than H_2SO_4, NH_3 and water.

420 Larger particles, few nm and up, observed at SMEAR I, were formed out of the immediate vicinity of the site and grown during the airmass advection. Secondary aerosol formation from Kola emissions together with primary particle emissions impact the aerosol size distribution, clearly increasing the concentrations of particles in each size class, and therefore unavoidably also CCN concentrations. Detailed assessment of the contribution of Kola SO_2 emissions to local and regional CCN concentrations and upscaling our results to cover the whole (sub)-arctic Eurasia with vastly polluting industrial cities such as Norilsk, require

425 more measurements – complemented by CCN or cloud residual measurements – ideally in more than only one location (SMEAR I) around the Kola peninsula, as well as regional chemical transport and aerosol dynamic modeling.

Data availability. Mass spectrometer and air ion spectrometer data related to this article are available upon request to the

430 corresponding author. Rest of the data are available for download from https://avaa.tdata.fi/web/smart/smear.

Supplement. The supplement related to this article is available online at:

Author contributions. MS designed the experiment, MS, NS, KN, TL, DK, SK, LB, TL, JL, PPA, PK, ES, PAR, and TJ

435 prepared the instruments, performed calibrations, collected the data and processed the data, MS and NS analyzed the data, EMD calculated the back trajectories. MS wrote the manuscript. All authors contributed to the interpretation of data and commented in manuscript.

Competing interests. The authors declare that they have no conflict of interest.

440

Acknowledgements. We thank GiGAS-UHEL calibration centre for at-site CI-APi-TOF calibration, Värriö research station staff for technical support and Lubna Dada for discussions related to sulphuric acid calculation.

Financial support. This work was supported by the Academy of Finland (projects: 296628, 328290, 310627, 334514), the
445 European Research Council (ERC) under the European Union's Horizon 2020 research and innovation programme (GASPARCON, grant agreement no. 714621) and the European Commission under the European Union's Horizon 2020 research and innovation programme (H2020-INFRADEV-2019-2, ACTRIS-IMP, grant Agreement no. 871115).

References

Aalto, P., Hämeri, K., Becker, E., Weber, R., Salm, J., Mäkelä, J. M., Hoell, C., O'Dowd, C. D., Karlsson, H., Hansson, H.-
450 C., Väkevä, M., Koponen, I. K., Buzorius, G., and Kulmala, M.: Physical characterization of aerosol particles during nucleation events, Tellus, 53B, 344–358, 2001.

Aitken, J. (1900). On some Nuclei of Cloudy Condensation. Transactions of the Royal Society of Edinburgh, 39(1), 15-25. doi:10.1017/S0080456800034025.
455

Almeida, J., Schobesberger, S., Kürten, A., Ortega, I. K., Kupiainen-Määttä, O., Praplan, A. P., Adamov, A., Amorim, A.,Bianchi, F., Breitenlechner, M., David, A., Dommen, J., Don-ahue, N. M., Downard, A., Dunne, E., Duplissy, J., Ehrhart, S.,Flagan, R. C., Franchin, A., Guida, R., Hakala, J., Hansel, A., Heinritzi, M., Henschel, H., Jokinen, T., Junninen, H., Kajos, M.,Kangasluoma, J., Keskinen, H., Kupc, A., Kurtén, T., Kvashin,A. N., Laaksonen, A., Lehtipalo, K.,
460 Leiminger, M., Leppä,J., Loukonen, V., Makhmutov, V., Mathot, S., McGrath, M. J.,Nieminen, T., Olenius, T., Onnela, A., Petäjä, T., Riccobono, F.,Riipinen, I., Rissanen, M., Rondo, L., Ruuskanen, T., Santos, F.D., Sarnela, N., Schallhart, S., Schnitzhofer, R., Seinfeld, J. H.,Simon, M., Sipilä, M., Stozhkov, Y., Stratmann, F., Tomé, A.,Tröstl, J., Tsagkogeorgas, G., Vaattovaara, P., Viisanen, Y., Vir-tanen, A., Vrtala, A., Wagner, P. E., Weingartner, E., Wex, H.,Williamson, C., Wimmer, D., Ye, P., Yli-Juuti, T., Carslaw, K.S., Kulmala, M., Curtius, J., Baltensperger, U., Worsnop,
465 D. R.,Vehkamäki, H., and Kirkby, J: Molecular understanding of sulphuric acid - amine particle nucleation in the atmosphere, Nature, 502, 359–363, https://doi.org/10.1038/nature12663, 2013.

Ball, S. M., Hanson, D. R., Eisele, F. L., and McMurry, P. H.: Laboratory studies of particle nucleation: Initial results for H2SO4, H2O, and NH3 vapors, J. Geophys. Res., 104, 23709–23718, doi:10.1029/1999JD900411, 1999.
470

Baccarini, A., Karlsson, L., Dommen, J., Duplessis, P., Vüllers, J., Brooks, I. M., Saiz-Lopez, A., Salter, M., Tjernström, M., Baltensperger, U., Zieger, P., and Schmale J.: Frequent new particle formation over the high Arctic pack ice by enhanced iodine emissions. Nat Commun. 11, 4924-. https://doi.org/10.1038/s41467-020-18551-0, 2020.

475   Bianchi, F., Trostl, J., Junninen, H., Frege, C., Henne, S., Hoyle,C. R., Molteni, U., Herrmann, E., Adamov, A., Bukowiecki, N.,Chen, X., Duplissy, J., Gysel, M., Hutterli, M., Kangasluoma, J.,Kontkanen, J., Kürten, A., Manninen, H. E., Münch, S., Peräkylä,O., Petäjä, T., Rondo, L., Williamson, C., Weingartner, E., Cur-tius, J., Worsnop, D. R., Kulmala, M., Dommen, J., and Baltensperger, U.: New particle formation in the free troposphere: A question of chemistry and timing, Science, 352, 1109–1112,https://doi.org/10.1126/science.aad5456, 2016.

480

Ehn, M., Thornton, J., Kleist, E., Sipilä, M., Junninen, H.,Pullinen, I., Springer, M., Rubach, F., Tillmann, R., Lee, B.,Lopez-Hilfiker, F., Andres, S., Acir, I.-H., Rissanen, M., Joki-nen, T., Schobesberger, S., Kangasluoma, J., Kontkanen, J., Nieminen, T., Kurtén, T., Nielsen, L. B., Jørgensen, S., Kjaer-gaard, H. G., Canagaratna, M., Maso, M. D., Berndt, T., Petäjä, T., Wahner, A., Kerminen, V.-M., Kulmala, M., Worsnop,D. R., Wildt, J., and Mentel, T. F.: A

485   large source of low-volatility secondary organic aerosol, Nature, 506, 476–479, https://doi.org/10.1038/nature13032, 2014.

Eisele, F. L., Lovejoy, E. R., Kosciuch, E., Moore, K. F., Mauldin III, R. L., Smith, J. N., McMurry, P. H., and Iida, K.: Negative atmospheric ions and their potential role in ion-induced nucleation, J. Geophys. Res., 111, D04305, doi:10.1029/2005JD006568, 2006.

490

Ekimov S.V., Samodova I.V., Petrov I.M., Troitsky V.V., and Burstein M.A.: Russian smelter emissions, Mining Journal, London, November 23, p. 393, 2001.

Gordon, H., Kirkby, J., Baltensperger, U., et al.: Causes and importance of new particle formation in the present-day and

495   preindustrial atmospheres, J. Geophys. Res.-Atmos., 122, 8739–8760, https://doi.org/10.1002/2017JD026844, 2017.

Hanson, D. R. and Eisele, F. L.: Measurement of prenucleation molecular clusters in the NH$_3$, H$_2$SO$_4$, H$_2$O system, J. Geophys. Res., 107, 4158, doi:10.1029/2001JD001100, 2002.

500   Hari, P., Kulmala, M., Pohja, T., Lahti, T., Siivola, E., Palva, L., Aalto, P., Hämeri, K., Vesala, T., Luoma, S., and Pulliainen, E.: Air pollution in eastern Lapland: challenge for an environmental research station, Silva Fenn., 28, 29–39, 1994.

Helsinki Region Environmental Services Authority, 2020.

505
    Jokinen, T., Sipilä, M., Junninen, H., Ehn, M., Lönn, G., Hakala,J., Petäjä, T., Mauldin III, R. L., Kulmala, M., and
    Worsnop, D. R.: Atmospheric sulphuric acid and neutral cluster measurements using CI-APi-TOF, Atmos. Chem. Phys., 12,
    4117–4125, doi:10.5194/acp-12-4117-2012, 2012.

510
    Jokinen, T., Sipilä, M., Kontkanen, J., Vakkari, V., Tisler, P., Du-plissy, E.-M., Junninen, H., Kangasluoma, J., Manninen,
    H. E., Petäjä, T., Kulmala, M., Worsnop, D. R., Kirkby, J., Virkkula, A.,and Kerminen, V.-M.: Ion-induced sulphuric acid–
    ammonia nu-cleation drives particle formation in coastal Antarctica, Sci. Adv.,4, eaat9744,
    https://doi.org/10.1126/sciadv.aat9744, 2018.

515
    Junninen, H., Ehn, M., Petäjä, T., Luosujärvi, L., Kotiaho, T., Kos-tiainen, R., Rohner, U., Gonin, M., Fuhrer, K., Kulmala,
    M., and Worsnop, D. R.: A high-resolution mass spectrometer to measure atmospheric ion composition, Atmos. Meas.
    Tech., 3, 1039–1053, doi:10.5194/amt-3-1039-2010, 2010.

    https://julkaisu.hsy.fi/ilmanlaatu-paakaupunkiseudulla-vuonna-2019-1.html#cLhM3ZB0tQ
520
    Kirkby, J., Curtius, J., Almeida, J., Dunne, E., Duplissy, J., Ehrhart, S., Franchin, A., Gagne, S.,Ickes, L., Kürten, A.,
    Kupc,A., Metzger, A., Riccobono, F., Rondo, L., Schobesberger,S., Tsagkogeorgas, G., Wimmer, D., Amorim,
    A., Bianchi,F., Breitenlechner, M., David, A., Dommen, J.,Downard,A., Ehn, M., Flagan, R. C., Haider, S., Hansel,
    A., Hauser, D., Jud, W., Junninen, H., Kreissl, F., Kvashin, A., Laaksonen, A., Lehtipalo, K., Lima, J., Lovejoy, E. R.,
525
    Makhmutov, V., Mathot, S., Mikkila, J., Minginette, P., Mogo, S., Nieminen, T., Onnela, A., Pereira, P., Petäjä,
    T.,Schnitzhofer,R.,Seinfeld, J. H., Sipilä, M., Stozhkov, Y., Stratmann,F., Tome, A., Vanhanen, J., Viisanen, Y.,Vrtala,
    A., Wagner, P. E., Walther, H., Weingartner, E., Wex, H., Winkler, P. M., Carslaw, K. S., Worsnop, D. R., Baltensperger,
    U., and Kulmala, M.: Role of sulphuric acid, ammonia and galactic cosmic rays in atmospheric aerosol nucleation., Nature,
    476,429–433, doi:10.1038/nature10343, 2011.

530
    Kirkby, J., Duplissy, J., Sengupta, K., Frege, C., Gordon, H.,Williamson, C., Heinritzi, M., Simon, M., Yan, C.,
    Almeida, J.,Tröstl, J., Nieminen, T., Ortega, I. K., Wagner, R., Adamov, A.,Amorim, A., Bernhammer, A.-K., Bianchi,
    F., Breitenlechner, M., Brilke, S., Chen, X., Craven, J., Dias, A., Ehrhart, S., Flagan,R. C., Franchin, A., Fuchs, C., Guida,
    R., Hakala, J., Hoyle, C.R., Jokinen, T., Junninen, H., Kangasluoma, J., Kim, J., Krapf,M., Kürten, A., Laaksonen, A.,
535
    Lehtipalo, K., Makhmutov, V., Mathot, S., Molteni, U., Onnela, A., Peräkylä, O., Piel, F., Petäjä, T., Praplan, A. P., Pringle,
    K., Rap, A., Richards, N. A. D., Riipinen, I., Rissanen, M. P., Rondo, L., Sarnela, N., Schobesberger, S., Scott, C. E.,
    Seinfeld, J. H., Sipilä, M., Steiner, G., Stozhkov,Y., Stratmann, F., Tomé, A., Virtanen, A., Vogel, A. L., Wagner, A.,
    Wagner, P. E., Weingartner, E., Wimmer, D., Winkler, P. M., Ye, P., Zhang, X., Hansel, A., Dommen, J., Donahue, N.M.,

Worsnop, D. R., Baltensperger, U., Kulmala, M., Carslaw, K.S., and Curtius, J.: Ion-induced nucleation of pure biogenic particles, Nature, 533, 521–526, https://doi.org/10.1038/nature17953, 2016.

Kulmala, M., Kontkanen, J., Junninen, H., Lehtipalo, K., Manni-nen, H. E., Nieminen, T., Petäjä, T., Sipilä, M., Schobesberger,S., Rantala, P., Franchin, A., Jokinen, T., Järvinen, E., Äijälä, M.,Kangasluoma, J., Hakala, J., Aalto, P. P., Paasonen, P., Mikkilä,J., Vanhanen, J., Aalto, J., Hakola, H., Makkonen, U., Ruuskanen, T., Mauldin, R. L., Duplissy, J., Vehkamäki, H., Bäck, J., Kortelainen, A., Riipinen, I., Kurten, T., Johnston, M. V., Smith, J. N., Ehn, M., Mentel, T. F., Lehtinen, K. E. J., Laaksonen, A., Kerminen, V.-M., and Worsnop, D. R.: Direct Observations of Atmospheric Aerosol Nucleation, Science, 339, 943–946, https://doi.org/10.1126/science.1227385, 2013.

Kürten, A., Rondo, L., Ehrhart, S., and Curtius, J.: Calibration of a chemical ionization mass spectrometer for the measurement of gaseous sulfuric acid, J. Phys. Chem. A, 116, 6375–6386, doi:10.1021/jp212123n, 2012.

Kürten, A., Jokinen, T., Simon, M., Sipilä, M., Sarnela, N., Junninen, H., Adamov, A., Almeida, J., Amorim, A., Bianchi, F., Breitenlechner, M., Dommen, J., Donahue, N. M., Duplissy, J., Ehrhart, S., Flagan, R. C., Franchin, A., Hakala, J., Hansel, A., Heinritzi, M., Hutterli, M., Kangasluoma, J., Kirkby, J., Laaksonen, A., Lehtipalo, K., Leiminger, M., Makhmutov, V., Mathot, S., Onnela, A., Petäjä, T., Praplan, A. P., Riccobono, F., Rissanen, M. P., Rondo, L., Schobesberger, S., Seinfeld, J. H., Steiner, G., Tomé, A., Tröstl, J., Winkler, P. M., Williamson, C., Wimmer, D., Ye, P., Baltensperger, U., Carslaw, K. S., Kulmala, M., Worsnop, D. R., and Curtius, J.: Neutral molecular cluster formation of sulfuric acid-dimethylamine observed in real-time under atmospheric conditions, P. Natl. Acad. Sci. USA, 111, 15019–15024, https://doi.org/10.1073/pnas.1404853111, 2014.

Kyrö, E.-M. Väänänen, R., Kerminen, V.-M., Virkkula, A., Petäjä, T., Asmi, A., Dal Maso, M., Nieminen, T., Juhola, S.,Shcherbinin, A., Riipinen, I., Lehtipalo, K., Keronen, P., Aalto,P. P., Hari, P., and Kulmala, M.: Trends in new particle forma-tion in eastern Lapland, Finland: effect of decreasing sulfur emis-sions from Kola Peninsula. Atmos. Chem. Phys., 14, 4383–4396, https://doi.org/10.5194/acp-14-4383-2014, 2014.

Mauldin III, R. L., Berndt, T., Sipilä, M., Paasonen, P., Petäjä, T.,Kim, S., Kurtén, T., Stratmann, F., Kerminen, V.-M., and Kulmala, M.: A new atmospherically relevant oxidant, Nature, 488,193–196, doi:10.1038/nature11278, 2012.

Merikanto, J., Spracklen, D. V., Mann, G. W., Pickering, S. J., and Carslaw, K. S.: Impact of nucleation on global CCN, Atmos. Chem. Phys., 9, 8601–8616, doi:10.5194/acp-9-8601-2009, 2009.

Mirme, S. and Mirme, A.: The mathematical principles and design of the NAIS – a spectrometer for the measurement of cluster ionand nanometer aerosol size distributions, Atmos. Meas. Tech., 6, 1061–1071, doi:10.5194/amt-6-1061-2013, 2013.

575

Paatero, J., Dauvalter, V., Derome, J., Lehto, J., Pasanen, J., Vesala, T., Miettinen, J., Makkonen, U., Kyrö, E.-M., Jernström, J., Isaeva, L., and Derome, K.: Effects of Kola air pollution on the environment in the western part of the Kola peninsula and Finnish Laplad: final report, Finnish Meteorological Institute Reports, 6, 1–26, 2008.

580 Rose, C., Zha, Q., Dada, L., Yan, C., Lehtipalo, K., Junninen, H., Mazon, S. B., Jokinen, T., Sarnela, N., Sipilä, M., Petäjä, T., Kerminen, V.-M., Bianchi, F., and Kulmala, M.: Observations of biogenic ion-induced cluster formation in the atmosphere, Sci. Adv.,4, 5218, https://doi.org/10.1126/sciadv.aar5218, 2018.

Schobesberger, S., Franchin, A., Bianchi, F., Rondo, L., Duplissy, J., Kürten, A., Ortega, I. K., Metzger, A., Schnitzhofer, 585 R., Almeida, J., Amorim, A., Dommen, J., Dunne, E. M., Ehn, M., Gagné, S., Ickes, L., Junninen, H., Hansel, A., Kerminen, V.-M., Kirkby, J., Kupc, A., Laaksonen, A., Lehtipalo, K., Mathot, S., Onnela, A., Petäjä, T., Riccobono, F., Santos, F. D., Sipilä, M., Tomé, A., Tsagkogeorgas, G., Viisanen, Y., Wagner, P. E., Wimmer, D., Curtius, J., Donahue, N. M., Baltensperger, U., Kulmala, M., and Worsnop, D. R.: On the composition of ammonia-sulfuric-acid ion clusters during aerosol particle formation, Atmos. Chem. Phys., 15, 55–78, doi:10.5194/acp-15-55-2015, 2015.

590

Solarin, S.A., Tiwari, A.: Convergence in Sulphur Dioxide (SO_2) Emissions Since 1850 in OECD Countries: Evidence from a New Panel Unit Root Test. Environ Model Assess 25, 665–675, https://doi.org/10.1007/s10666-019-09687-5, 2020.

Sipilä, M., Sarnela, N., Jokinen, T., Henschel, H., Junninen, H., Kontkanen, J., Richters, S., Kangasluoma, J., Franchin, A., 595 Peräkylä, O., Rissanen, M. P., Ehn, M., Vehkamäki, H., Kurten, T., Berndt, T., Petäjä, T., Worsnop, D., Ceburnis, D., Kerminen, V.-M., Kulmala, M., and O'Dowd, C.: Molecular-scale evidence of aerosol particle formation via sequential addition of HIO3, Nature, 537, 532–534, https://doi.org/10.1038/nature19314, 2016.

Stein, A. F., R. R. Draxler, G. D. Rolph, B. J. B. Stunder, M. D. Cohen, and F. Ngan, 2015: NOAA's HYSPLIT 600 Atmospheric Transport and Dispersion Modeling System. Bull. Amer. Meteor. Soc., 96, 2059–2077, https://doi.org/10.1175/BAMS-D-14-00110.1.

Tammet, H., Hõrrak, U., Laakso, L., and Kulmala, M.: Factors of air ion balance in a coniferous forest according to measure-ments in Hyytiälä, Finland, Atmos. Chem. Phys., 6, 3377–3390, doi:10.5194/acp-6-3377-2006, 2006.

605

Tuovinen J.-P., Laurila, T., and Lättilä H.: Impact of the sulphur dioxide sources in the Kola peninsula on air quality in northernmost Europe, Atmospheric Environment, 27A, No. 9, 1379-1395, 1993.

Vehkamäki, H., McGrath, M. J., Kurtén, T., Julin, J., Lehtinen K.E.J., and Kulmala, M.: Rethinking the application of the
610 first nucleation theorem to particle formation. J. Chem. Phys. 136, 094107, https://doi.org/10.1063/1.3689227, 2012.

Wang , M , Kong , W , Marten , R , He , X-C , Chen , D , Pfeifer , J , Heitto , A , Kontkanen , J , Dada , L , Kuerten , A , Yli-Juuti , T , Manninen , H E , Amanatidis , S , Amorim , A , Baalbaki , R , Baccarini , A , Bell , D M , Bertozzi , B , Braekling , S , Brilke , S , Murillo , L C , Chiu , R , Chu , B , De Menezes , L-P , Duplissy , J , Finkenzeller , H , Carracedo ,
615 L G , Granzin , M , Guida , R , Hansel , A , Hofbauer , V , Krechmer , J , Lehtipalo , K , Lamkaddam , H , Lampimaki , M , Lee , C P , Makhmutov , V , Marie , G , Mathot , S , Mauldin , R L , Mentler , B , Mueller , T , Onnela , A , Partoll , E , Petaja , T , Philippov , M , Pospisilova , V , Ranjithkumar , A , Rissanen , M , Rorup , B , Scholz , W , Shen , J , Simon , M , Sipila , M , Steiner , G , Stolzenburg , D , Tham , Y J , Tome , A , Wagner , A C , Wang , D S , Wang , Y , Weber , S K , Winkler , P M , Wlasits , P J , Wu , Y , Xiao , M , Ye , Q , Zauner-Wieczorek , M , Zhou , X , Volkamer , R , Riipinen , I ,
620 Dommen , J , Curtius , J , Baltensperger , U , Kulmala , M , Worsnop , D R , Kirkby , J , Seinfeld , J H , El-Haddad , I , Flagan , R C & Donahue , N M: Rapid growth of new atmospheric particles by nitric acid and ammonia condensation, Nature , 581 , 184-189, https://doi.org/10.1038/s41586-020-2270-4, 2020.

Weber, R. J., McMurry, P. H., Eisele, F. L., and Tanner, D. J.: Measurement of expected nucleation precursor species and 3-
625 500-nm diameter particles at Mauna Loa observatory, Hawaii, J. Atmos. Sci., 52, 2242–2257, 1995.

Wiedensohler, A., Birmili, W., Nowak, A., Sonntag, A., Weinhold, K., Merkel, M., Wehner, B., Tuch, T., Pfeifer, S., Fiebig, M., Fjäraa, A. M., Asmi, E., Sellegri, K., Depuy, R., Venzac, H., Vil lani, P., Laj, P., Aalto, P., Ogren, J. A., Swietlicki, E., Williams, P., Roldin, P., Quincey, P., Hüglin, C., Fierz-Schmidhauser, R., Gysel, M., Weingartner, E., Riccobono, F.,
630 Santos, S., Grüning, C., Faloon, K., Beddows, D., Harrison, R., Monahan, C., Jennings, S. G., O'Dowd, C. D., Marinoni, A., Horn, H.-G., Keck, L., Jiang, J., Scheckman, J., McMurry, P. H., Deng, Z., Zhao, C. S., Moerman, M., Henzing, B., de Leeuw, G., Löschau, G., and Bastian, S.: Mobility particle size spectrometers: harmonization of technical standards and data structure to facilitate high quality long-term observations of atmospheric particle number size distributions, Atmos. Meas. Tech., 5, 657–685, doi:10.5194/amt- 5-657-2012, 2012.
635

Yan, C., Dada, L., Rose, C., Jokinen, T., Nie, W., Schobesberger,S., Junninen, H., Lehtipalo, K., Sarnela, N., Makkonen, U., Gar-mash, O., Wang, Y., Zha, Q., Paasonen, P., Bianchi, F., Sipilä, M.,Ehn, M., Petäjä, T., Kerminen, V.-M., Worsnop, D. R., and Kul-mala, M.: The role of $H_2SO_4-NH_3$ anion clusters in ion-inducedaerosol nucleation mechanisms in the boreal forest, Atmos.Chem. Phys., 18, 13231–13243, https://doi.org/10.5194/acp-18-13231-2018, 2018.

640

Yao, L., Garmash, O., Bianchi, F., Zheng, J., Yan, C., Kontkanen, J., Junninen, H., Mazon, S. B., Ehn, M., Paasonen, P., Sipilä, M., Wang, M., Wang, X., Xiao, S., Chen, H., Lu, Y., Zhang, B., Wang, D., Fu, Q., Geng, F., Li, L., Wang, H., Qiao, L., Yang, X., Chen, J., Kerminen, V.-M., Petäjä, T., Worsnop, D. R., Kulmala, M., and Wang, L.: Atmospheric new particle formation from sulfuric acid and amines in a Chinese megacity, Science, 361, 278–281,

645   https://doi.org/10.1126/science.aao4839, 2018.

650

Figure 1. Map of the study area. Industrial cities of Nikel, Zapoljarnij, Monchegorsk, Kandalaksha have large scale metal smelters emitting vast quantities of SO₂ in the atmosphere. Kovdor and Olenegorsk mines produce nickel/iron ore but have no smelter
655   **industry. Kirovsk and Apatity are phosphate mining and prosessing sites.**
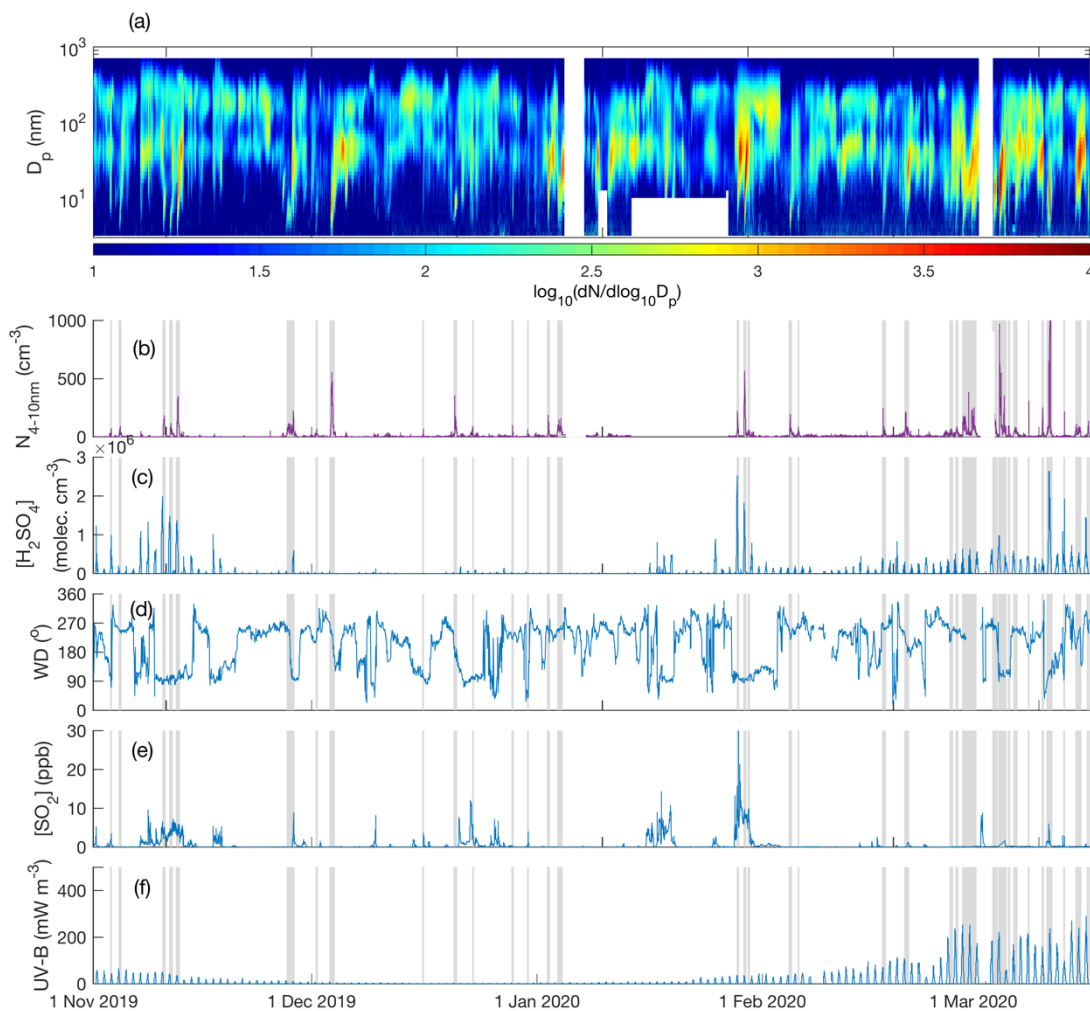
Figure 2. 5-month aerosol size distribution (a), small particle (4-10 nm) concentration (b), calculated sulphuric acid concentration (Dada et al., 2020) (c), wind direction (d), [SO₂] (e) and UV-B radiation (f) between 1.11.2019 – 31.3.2020. Gray shaded areas depict the times with observed < 10 nm new particle formation. Polar night (sun constantly below horizon) period is from Dec. 9th until Jan 4th.
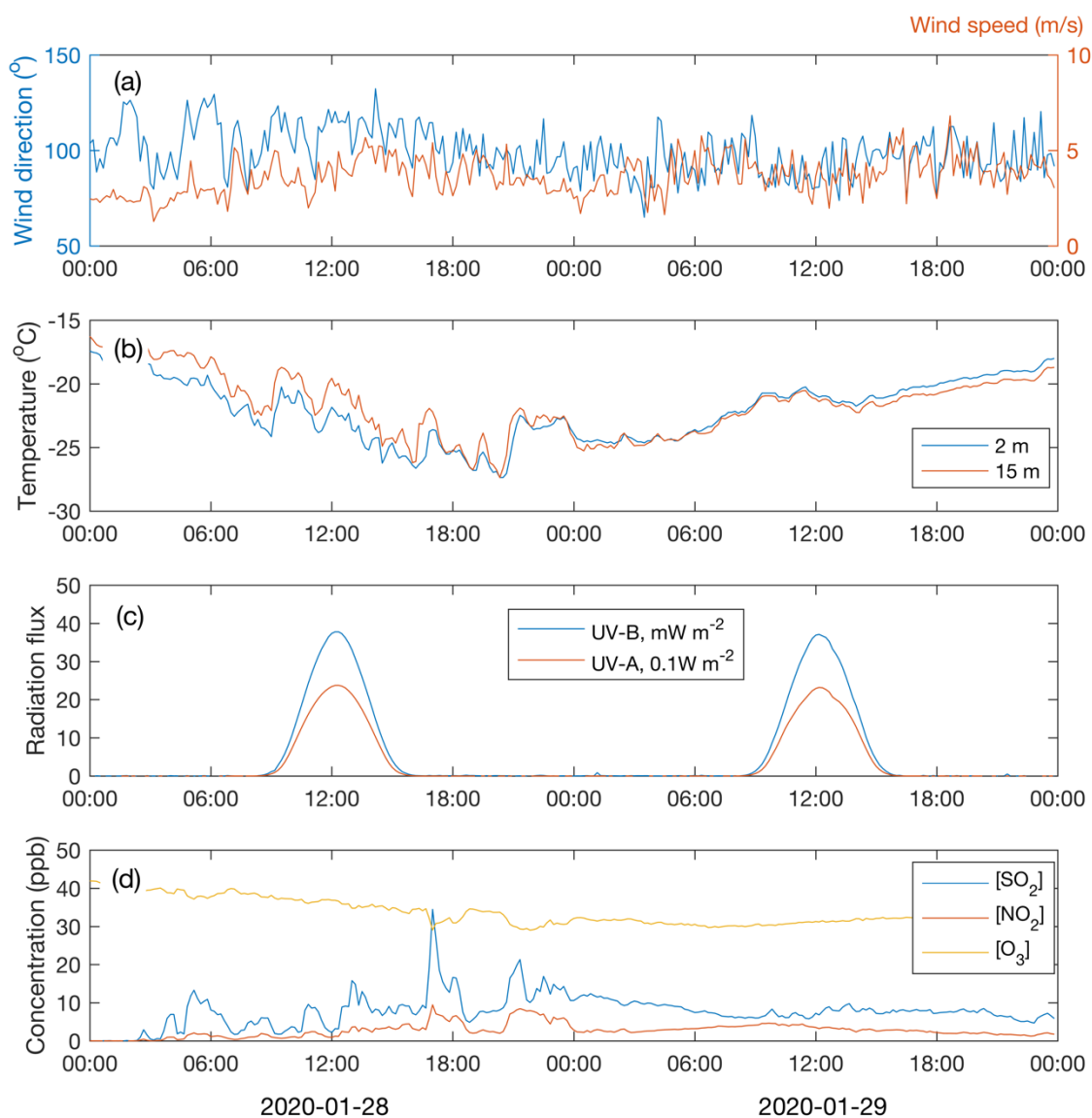
665

Figure 3. Wind speed and direction at 16 m height (a), air temperature at two heights (b) , UV-B and UVA radiation (c) and concentrations of SO₂, NO₂, O₃ (d) during the examination period.
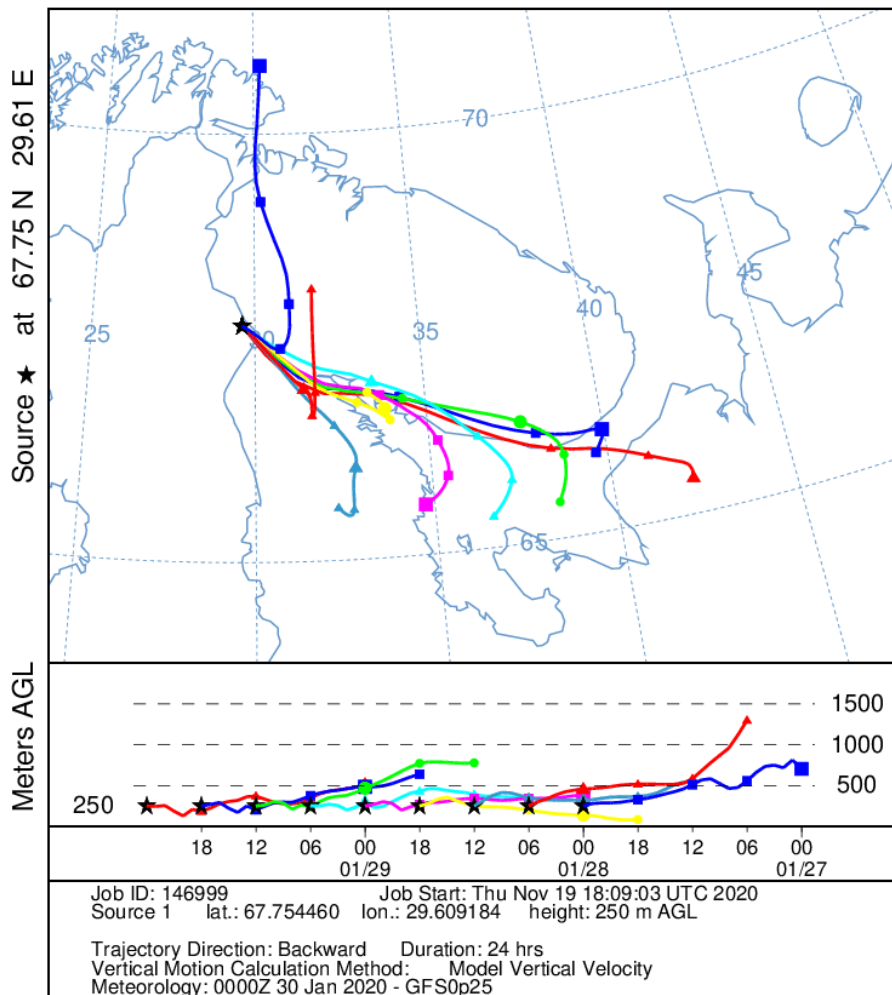
670

Figure 4. 24-hour back trajectories with arriving time between 28th January 00:00 and 30th January 00:00.
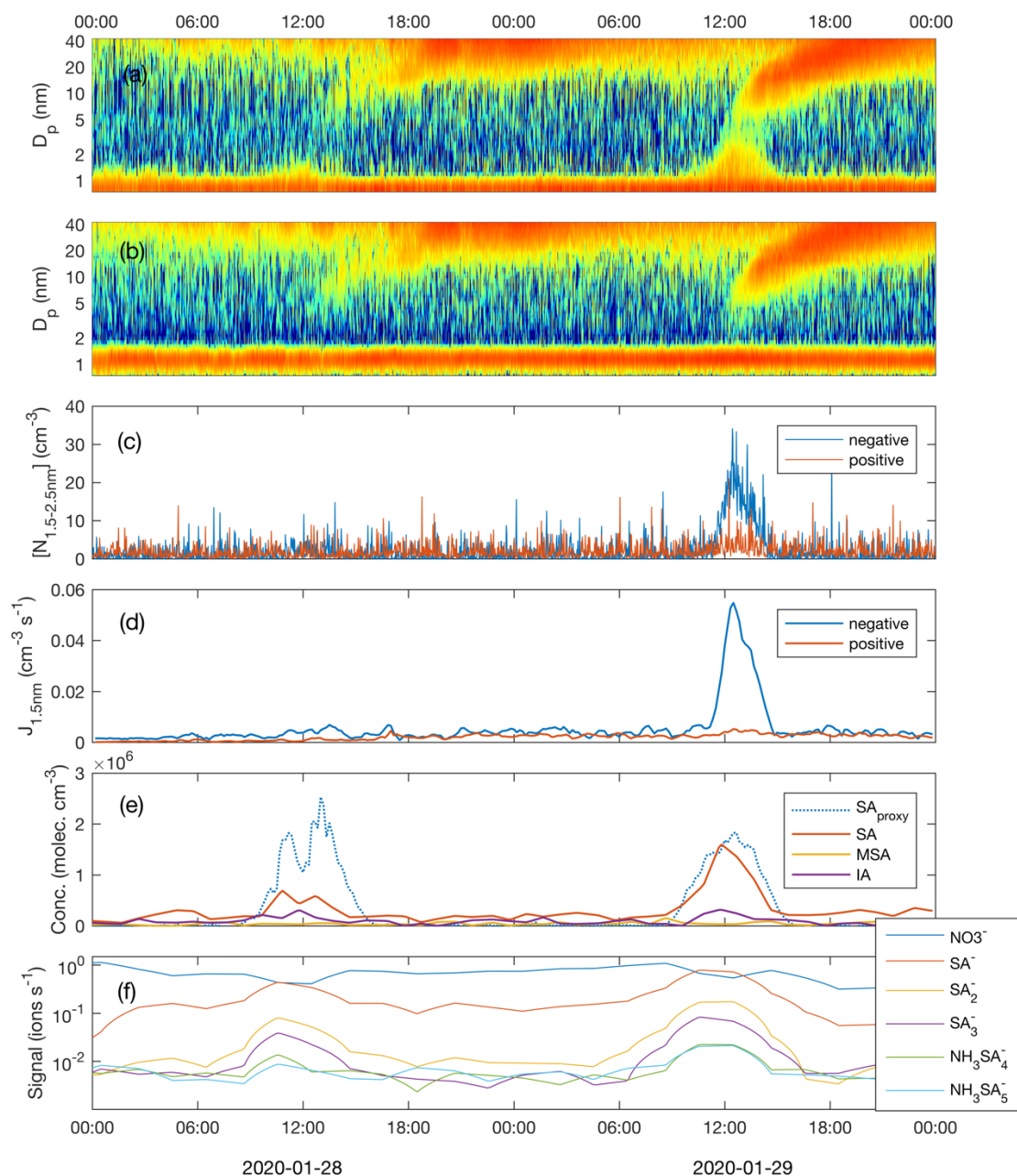
Figure 5. Size distribution of negative (a) and positive (b) clusters and particles, concentration of freshly nucleated, charged 1.5-2.5 nm clusters (c), formation rate of negative and positive 1.5 nm clusters (d) measured concentrations of sulphuric acid (H₂SO₄), methane sulphonic acid (MSA) and iodic acid (HIO₃) as well as sulphuric acid concentration estimated by proxy calculation (e) and signal intensity of nucleating ion clusters with different composition (f) during the examination period.

680
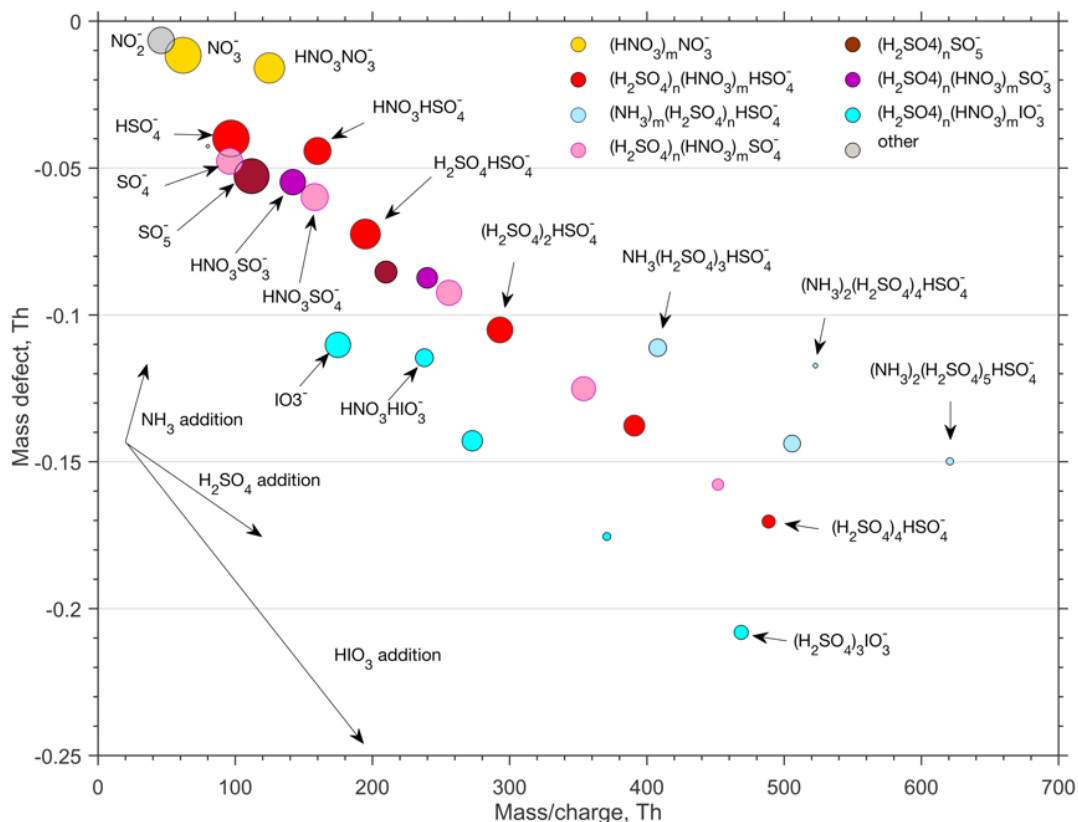
Figure 6. Mass defect plot (with 2 h effective integration time) on anion cluster distribution recorded by APi-TOF during intensive
685 **cluster formation on 29th of January 2020. See text for detailed description.**
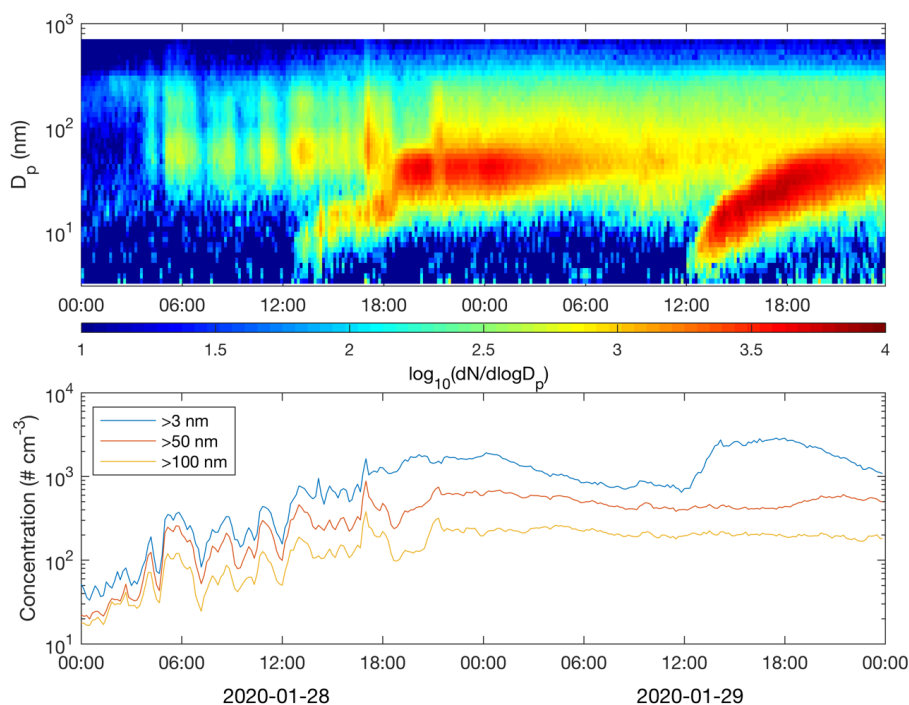
Figure 7. Particle number size distribution (a) and concentrations of particles larger than 3 nm, 50 nm and 100 nm (b) recorded by DMPS.
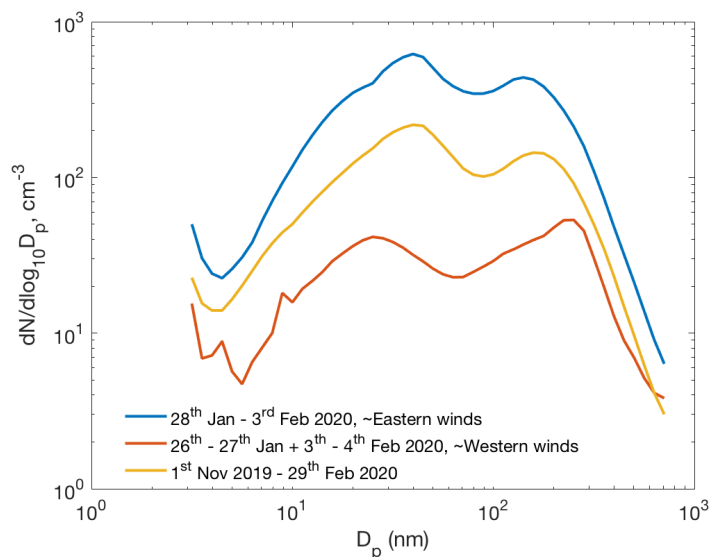
Figure 8. Average particle number size distributions during the ca. 1-week period of eastern winds (28th Jan – 3rd Feb 2020), during the preceding and succeeding time period with western winds and average number size distribution between 1st November and 29th February. New particle formation in the eastern airmass significantly increases the concentrations of particles in every size class.